Deep Sea Research Part I: Oceanographic Research Papers
August 2014, Volume 90, Pages 62-75
http://dx.doi.org/10.1016/j.dsr.2014.04.004

High-resolution dynamics of a deep-sea Hydrothermal mussel assemblage monitored by the EMSO-Açores MoMAR observatory

J. Sarrazin[a], D. Cuvelier[a], L. Peton[b], P. Legendre[c], P.M. Sarradin[a]

[a] Institut Carnot Ifremer EDROME, Centre de Bretagne, REM/EEP, Laboratoire Environnement Profond, F-29280 Plouzané, France
[b] UFR Sciences et Techniques, 2 rue de la Houssinière, 44322, Nantes, cedex 3, France
[c] Département de Sciences Biologiques, Université de Montréal, C.P. 6128, succursale Centre-ville, Montréal, Québec H3C 3J7, Canada

Abstract:

Although the spatial distribution of hydrothermal vent assemblages in relation to environmental conditions has been assessed in several studies, there is little documented data on the temporal variation of the fauna and corresponding abiotic factors in a vent community. Here, we present one of the longest integrated (faunal and environmental data) time series ever obtained in a hydrothermal ecosystem. The data were acquired using the TEMPO ecological module that was deployed between 2006 and 2008 on the Mid-Atlantic Ridge, providing the first insights into the day-to-day variations in a *Bathymodiolus azoricus* mussel assemblage from the Lucky Strike vent field for the 48 days during which the video camera operated. The time-series yielded additional valuable information on longer-term variation in faunal distribution (comparing~2 years), temperature (11.7 months) and iron concentrations (3.8 months).

Results from daily observations showed that the vent mussel assemblage was quite stable over the 48 days of the study, reflecting the relative stability of environmental conditions during this period. *Bathymodiolus azoricus* mussels appeared to thrive in areas of very limited hydrothermal fluid input in habitats that are, as in other deep-sea ecosystems, significantly influenced by ocean tidal signals. Variation in species abundance was observed but, with the exception of *Mirocaris fortunata* shrimp, no links could be established with measured environmental variables. Although we did not observe any clear tidal influence on vent fauna, it is likely that physiological processes and species' activities are influenced by these periodic variations. Longer time series are currently being acquired by different experiments deployed on the EMSO-Açores MoMAR observatory (2010–2013 and still recording). They should further improve our knowledge of the dynamics of hydrothermal systems and their associated faunal communities.

Highlights

► Relative stability of the vent mussel assemblage in relation with abiotic conditions. ► Hydrothermal habitats significantly influenced by ocean tidal signals. ► Temporal variations in species abundance observed. ► No established links between faunal abundance (except for shrimp) and environmental variables. ► Direct species interactions not frequently observed.

Keywords : Hydrothermal vents ; Faunal dynamics ; Mid-Atlantic Ridge ; Deep-sea observatory ; *Bathymodiolus azoricus* mussel assemblages ; Sulphide edifices ; Environmental conditions

1. Introduction

Over the past 20 years, three major vent fields located in the northern part of the Mid-Atlantic Ridge (MAR), south of the Azores, have been repeatedly studied during oceanographic cruises involving international research teams. The Menez Gwen, Lucky Strike and Rainbow hydrothermal fields encompass different depth ranges and are characterised by the presence of different geological substrata and contrasting fluid chemistries (Fouquet et al., 1995 and Charlou et al., 2000). Within these fields, Lucky Strike (LS) was selected for the deployment of one of the first deep-sea observatories (Cannat et al.,

2011; Colaço et al., 2011). Part of this hydrothermally active zone is located within a Portuguese Marine Protected Area (Santos et al., 2003) that includes different types of marine ecosystems such as hydrothermal vents, seamounts and cold-water corals.

As in many hydrothermal ecosystems, the faunal assemblages of the LS vent field are distributed in mosaics spread across the various active sulphide edifices (Van Dover et al., 1996; Desbruyères et al., 2000, 2001). Two types of faunal associations are important in the LS field: the assemblages visually dominated by the vent mussel *Bathymodiolus azoricus* and one faunal assemblage visually dominated by the alvinocaridid shrimp *Mirocaris fortunata* (De Busserolles et al., 2009; Cuvelier et al., 2009, 2011a). Over the past few years, we have shown that the structure and composition of these assemblages are controlled by their positions in the mixing zone located between the hot hydrothermal fluids and cold surrounding seawater (Cuvelier et al., 2009; Sarradin et al., 2009). The mussel assemblages are found in the colder microhabitats (4.4-6.1°C) of the ecosystem whereas the shrimp assemblages colonise slightly warmer microhabitats (5.2-9.5°C), their temperature niche overlapping slightly with that of mussels (Cuvelier et al., 2011a). The environmental conditions found in the different vent habitats have a significant impact on microbial production because they influence the availability of energy sources (De Busserolles et al., 2009) and cause modifications in the proportion of endosymbionts in *B. azoricus* gills (Halary et al., 2008). In addition, they significantly influence the bioavailability of potentially toxic compounds such as sulphides and heavy metals (Cosson et al., 2008; Sarradin et al., 2009). The role of abiotic factors in controlling the structure and functioning of vent communities at the scale of a single edifice in this vent field was recently evaluated using multivariate analyses, and supplemented with biodiversity studies encompassing the meiofaunal

compartment (De Busserolles et al., 2009; Cuvelier et al., 2011a, Sarrazin et al. unpublished data). In addition, long-term colonisation experiments have been initiated to obtain information on the role of hydrothermal activity in colonisation processes and species diversity (Cuvelier et al., 2014).

While the spatial distribution of hydrothermal fauna is slowly being brought to light (Fisher et al., 1988; Sarrazin et al., 1997, 1999; Shank et al., 1998; Desbruyères et al., 2001; Luther et al., 2001; Cuvelier et al., 2011a; Marsh et al., 2012; Nye et al., 2013), there are very limited data on the temporal variation of vent communities and the corresponding abiotic factors (Glover et al., 2010; Tokeshi, 2011). Most temporal ecological studies at vents investigate recolonisation processes after disruptive events on fast and moderately spreading ridges (Tunnicliffe et al., 1997; Shank et al., 1998; Tsurumi and Tunnicliffe 2001; Shank et al., 2003; Nees et al., 2008; Marcus et al., 2009) and are based on yearly cruises rather than on continuous monitoring. A few studies have used time-series measurements at vents to monitor structural changes and variation of particle loads in low temperature hydrothermal deposit (Johnson and Tunnicliffe, 1985, 1988) and describe tubeworm behaviour (Tunnicliffe et al. 1990). Submersibles have also been used to acquire images at yearly intervals to follow variations in faunal distribution with the evolution of geological structures, observing the response of faunal assemblages to environmental changes or catastrophic events (landslide, cessation of venting, etc.) in specific areas (Van Dover, 1995; Sarrazin et al., 1997; Shank et al., 1998; Copley et al., 2007; Podowski et al., 2009; Gebruk et al., 2010; Cuvelier et al., 2011b). The effects of a drilling operation on a vent community have also been reported (Copley et al., 1997). Recently, a series of video images collected during 14 years of diving cruises on the LS vent field was used to evaluate the temporal

97 changes in the distribution of faunal assemblages on the Eiffel Tower edifice; it
98 demonstrated the relative overall stability on a decadal-scale (Cuvelier et al., 2011b). For the
99 same period, the study of seafloor image mosaics at LS indicate a general decline in diffuse
100 outflows throughout the vent field (Barreyre et al., 2012), although this could not be
101 corroborated for the Eiffel Tower edifice (Cuvelier et al., 2011b).
102
103 At the spatial scale of a single edifice, the temporal variability of temperature, used as a
104 proxy for hydrothermal inputs (Sarradin et al., 2009), has been investigated. Preliminary
105 results show that hydrodynamic processes and spatial localisation influence the variability in
106 recorded temperature data, suggesting that each microhabitat is constrained in space and
107 time (Cuvelier et al., 2011b). Nevertheless, because most oceanographic cruises in the
108 Azores region take place in the summer and operate over a short period of time, sub-annual
109 variation in faunal communities, the associated environmental conditions and their
110 interactions are difficult to assess. Therefore, knowledge about basic biological processes
111 such as reproduction, recruitment, biological rhythms and species interactions remains
112 limited.
113
114 The aim of the present study was to obtain basic knowledge about the day-to-day variation
115 in biotic and abiotic factors in a hydrothermal mussel assemblage on an active sulphide
116 edifice on the MAR, using data collected by the TEMPO temporal observatory module
117 (Sarrazin et al., 2007), and to examine the links between faunal and environmental
118 dynamics.
119

In the first part of the study, video images were used to evaluate changes in the structure of the monitored faunal assemblage at sub-annual scales. Video and screen-still images were analysed to identify the presence of biological rhythms and gain insights into species interactions. Imagery analysis of the fauna between the two years (2006-2008) was also carried out in order to assess variations at the deployment site. In the second part, video images and environmental monitoring data were coupled to examine the response of the fauna to variations in their habitats and in relation to catastrophic events. Temperature and total dissolved iron concentrations were used as proxies for hydrothermal inputs (Sarradin et al., 2009). The data collected have the potential to enhance our understanding of the temporal dynamics of hydrothermal ecosystems at sub-annual scales.

2. Materials and methods

2.1. Study site

The LS vent field is a well-known field with a central lava lake surrounded by more than 20 active hydrothermal edifices (Fouquet et al., 1995; Ondreas et al., 2009; Fig. 1). In the south-eastern section of the field, the Eiffel Tower hydrothermal edifice is an 11 m high structure. It is one of the most visited sites in the vent field, and has been the subject of several ecological studies (Desbruyères et al., 2000, 2001; Colaço et al., 2002; De Busserolles et al., 2009; Cuvelier et al., 2009; 2011a, b, 2012, 2014). The base of the Eiffel Tower edifice was extensively monitored during the MoMARETO 2006 cruise and deemed suitable for deployment of the MoMAR interdisciplinary deep-sea observatory. Primarily operated by French research teams, MoMAR is an international programme whose objective is to monitor hydrothermal vent processes at the MAR (37°18'N, ~200 km south of the Azores).

144 This observatory combines long-term observations, detailed site studies and experimental
145 work and includes a variety of seafloor and water column sensors. A subset of the data is
146 periodically transmitted to a relay buoy moored nearby and then onshore via satellite.
147 MoMAR has been active since 2006, with yearly maintenance cruises and regular upgrades
148 (Cannat et al., 2011). It recently joined the EMSO European programme as the *EMSO-Açores*
149 *observatory* (www.emso-eu.org).
150

151 **2.2. The TEMPO ecological module**

152 A prototype of the TEMPO ecological module (Sarrazin et al., 2007) was first deployed
153 during the MoMARETO 2006 cruise at the LS vent field using the remotely operated vehicle
154 (ROV) *Victor6000*. This prototype was composed of two main structures. The first one
155 hosted the master electronics and the power supply (SEAMON, Blandin and Rolin, 2005).
156 This SEAMON seabed station was used to support a local set of sensors, providing them with
157 data storage, communication channels and power (8 kWh). The second structure (or sensor
158 module) was moored jointly with the first one and was connected to the main module by a
159 15 m long cable. It was built on an aluminium frame (0.85 x 0.70 x 0.65 cm) equipped with
160 two adjustable feet and was handled by the submersible arm. The module was composed of
161 an autonomous video camera (720 x 576 pixels) and two 35 W LED projectors, both
162 protected by an anti-fouling system based on local chlorine generation. It also included a
163 CHEMINI Fe *in situ* analyser (Vuillemin et al., 2009; measuring total dissolved iron
164 concentrations, called Fe hereafter), along with autonomous temperature probes (NKE,
165 ST6000). During deployment of TEMPO, SEAMON communicated with the ROV via a
166 contact-less serial interface (CLSI) and transmitted still images, allowing for optimal
167 positioning of the camera view and the related environmental sensors.

168

169 During the 2006 deployment cruise, we dedicated considerable dive time to find the ideal
170 location for the ~1 m^3 TEMPO module. This location had to fulfil four requirements: a nearly
171 flat area to position the module, the presence of a living faunal assemblage, a fluid source in
172 the immediate vicinity (< 1 m), and accessibility for the ROV. After a few hours of surveying,
173 TEMPO was positioned at the base of the south-east side of the Eiffel Tower edifice. A ledge
174 colonised by *Bathymodiolus azoricus* mussels, featuring a diffuse flow zone with visible
175 shimmering water was chosen for the temporal study (Fig. 2).

176

177 The camera was programmed to record 4 min of video footage twice a day along with
178 temperature measurements every hour and Fe measurements every 12 h. TEMPO recorded
179 data onto a hard disk drive for subsequent recovery of images (August 2008, MoMAR08
180 cruise with ROV *Victor6000*). The deployment calibration/set-up of the camera used more
181 power than expected and the batteries only lasted 48 days, instead of the 365 days initially
182 planned. In addition, although the module was initially programmed to record twice a day, it
183 recorded haphazardly: sometimes it recorded twice a day, sometimes only in the morning or
184 the evening, and sometimes it skipped a day or more. Overall, a total of 204 min (recorded
185 over 48 days) of video images was analysed. The temperature probes recorded data for the
186 whole duration of the mooring, and the CHEMINI Fe module operated for 4.37 months, i.e.
187 until complete consumption of the chemical reagents available. An overview of the faunal
188 and environmental data available for the duration of the video recordings (48 days) is shown
189 in Fig. 3. As the CHEMINI Fe module started recording with a 10 day delay, only 38 days of
190 iron measurements were available for use in conjunction with video image analyses.

191

192 **2.3. TEMPO image analyses**

193 In a previous study of MAR hydrothermal ecosystems, several quantitative factors that can
194 be accurately assessed from video images were identified by conducting a comparison with
195 conventional faunal sampling (Cuvelier et al., 2012). These factors included the
196 identification and quantification of a limited number of macrofaunal species, as well as the
197 extraction of selected biological and environmental variables such as fluid flow rates,
198 microbial coverage and biological rhythms (Cuvelier et al. 2012). Video images in this study
199 were used to extract similar types of data.
200
201 *Abundance* – One still image of each video recording was used as a template to locate and
202 count the relatively sedentary animals (i.e. *B. azoricus* mussels and *Pseudorimula*
203 *midatlantica* limpets, Table 1). For the highly mobile shrimp species (*M. fortunata*), every 4
204 min of video recording was divided into 5 still images (start, 1 min, 2 min, 3 min, and end at
205 4 min). Twenty seconds of video footage was also investigated around these time stamps to
206 count the shrimp. For the *Segonzacia mesatlantica* crabs, the entire 4 min recording was
207 analysed and abundance was recorded (Table 1).
208
209 *Opened mussel valves* were counted in five still images (start, 1 min, 2 min, 3 min and end)
210 for each video recording (Table 1). Mussels were considered to have open valves when
211 either the exhalant siphon or an opening between the two valves was visible. Counts were
212 quantified as the percentage (%) of visible mussels with open valves. In addition, a random
213 selection of 22 video recordings were analysed in detail for changes in mussel valve opening
214 such as sudden closure reactions.
215

Microbial cover was assessed on a selection of 10 still images taken at 5 day intervals (Table 1). Microbial patches were manually marked in white and the rest of the image was filled in black. The percentage (%) of the image covered by microbial mats was then measured using the ImageJ image analysis software (Rasband et al., 2012).

Vertical and horizontal components of water movement were estimated from on-screen tracking of particles. The particles travelling upwards were used as a proxy for hydrothermal fluid flow while those moving sideways were used to estimate currents. The distance travelled over time ($cm \cdot s^{-1}$) was estimated and these values were subsequently transformed to numerical classes (Table 1). The video recordings in which no particles could be observed were compared to other video recordings (using visual indicators of flow such as turbulence, shimmering water, etc.) and placed in the most similar corresponding classes. Since not all velocities were effectively measured (some were estimated from images), we used categorical values (classes) instead of numerical values.

Video images recorded at 8:00 UTC were referred to as A.M. (morning) while those recorded at 20:00 UTC were referred to as P.M. (evening).

2.4. Analysis of high-definition photographs taken in 2006 and 2008

High-definition photographs taken during deployment (1 September 2006) and recovery (12 August 2008) of the TEMPO module by the ROV *Victor6000* were used to monitor long-term variation in faunal distribution (23.3 months) (Table 2). Two sets of photographs were selected: wide-angle views of the scene (taken by the ROV), and closer views, corresponding to the images recorded by the TEMPO camera. The surface covered by each of these

240 photographs was estimated using ImageJ with the length of the tip of the sampling inlet (29
241 mm) serving as a calibration reference (Fig. 2). The surface covered by mussels and
242 microbial mats was evaluated along with mussel, shrimp and crab densities. As described
243 above for the video still images, the surface covered by mussels and microbial mats was
244 manually marked in different colours and the percentage (%) of coverage was measured.
245

246 **2.5. Statistical analyses**

247 All statistical analyses were carried out in R (R Development Core Team, 2012). Pearson
248 correlations with permutation tests (999 permutations), a valid test in the absence of
249 normal error distribution, were calculated between all variables for the duration of the
250 video recordings to determine which variables of faunal abundances or environmental
251 factors showed similar or contrasting trends. Analyses of variance (ANOVA) with
252 permutation tests (999 permutations) were conducted for shrimp abundance and the
253 proportion of open mussel valves to examine how they changed within and between the
254 video recordings.
255

256 Short-term variations in temperature for the duration of the video recording were analysed
257 with correlograms. Rhythms and periodicities of temperature values and Fe measurements
258 over longer terms were examined using Whittaker-Robinson periodograms (Legendre,
259 2012). Prior to periodogram analyses, data were tested for stationarity. When that
260 condition was not met, a linear trend was extracted by regression to ensure stationarity and
261 residuals were used for periodogram analysis. Missing values in the dataset were indicated
262 by NA (not available). Whittaker-Robinson periodograms are based on a Buys-Ballot table,
263 which folds a time series into a table along a period with maximum length of n/2. Buys-

Ballot tables corresponding to periods of interest (e.g. diurnal cycles) can be constructed to test hypotheses (Legendre and Legendre, 2012). The statistic used in this function is the standard deviation of the means of the columns of the Buys-Ballot table (Enright, 1965 in Legendre and Legendre, 2012). However, some degree of caution is necessary to interpret the results of significance tests in Whittaker-Robinson periodograms because harmonics of a basic period are often also found to be significant. Periodograms were calculated for the time period for which images were available (48 days) as well as for the long environmental time series collected after image recordings stopped (>1 year).

3. Results

3.1. Data collected

Temperature and Fe data originating from the sampling inlet positioned within the camera's field of focus and on the mussel assemblage (Figs. 4A, B) were also used as explanatory variables of faunal variations. A 3 min delay was observed between temperature and Fe measurements, precluding any test of correlation of the two data sets as originally planned (Vuillemin et al., 2009). On day 25 following TEMPO deployment, the sampling inlet was repositioned after a disturbance by a chimaeroid fish, identified as a male *Hydrolagus pallidus*, which passed between the module and the monitored faunal assemblage. The event was captured by the TEMPO camera. From day 1 to day 25, the probe had been positioned on the mussel bed and after day 25, it slid downwards about 6 cm into the diffuse flow area. Due to the significant difference in measured temperatures (a difference of almost 3°C) (Fig. 4A), we considered these two periods as separate data sets for the statistical analyses.

The first temperature data set comprised days 1 to 25 (referred to as P1 from here on, 04/09/2006 to 29/09/2006); it was used as explanatory data in the study of faunal variation. Days 26 to 48 are referred to as P2 (29/09/2006 to 22/10/2006) corresponding to the second positioning of the probe until the end of the video recording. The P2 time series was not used for faunal interpretation (except for microbial mat coverage) because the inlet was no longer positioned on the studied assemblage. The third dataset (P3) featured the long-term time series of temperature values (22/10/2006 to 14/10/2007), adding up to 357 days (11.7 months). This period was used to determine significant periodicities in diffuse flow temperature. Unfortunately, the temperature data from August 2007 onwards could not be used because of a calibration problem.

As the *in situ* Fe analyser started recording with a ten-day delay and because the sampling probe slid at day 25, only 15 days of iron measurements were available for use in conjunction with image analyses (days 10 to 25 (P1), Fig. 3). The iron (Fe, Fig. 4B) data set spanned 133 days in total. 117 days, corresponding to 234 measurements in P2 and P3 -with 6 missing values- were considered for the study of long-term patterns.

3.2. Short-term variation

A total of 51 video recordings of 4 min each, spanning 48 days, were analysed. The scene filmed by TEMPO was characterised by the presence of three main areas with, from bottom to top: (1) a small diffusion zone with the presence of white anhydrites, (2) an elongated *B. azoricus* mussel assemblage bordered by (3) a rocky substrate with or without white microbial mats (Fig. 2). The sampling inlet (for temperature and Fe) was initially positioned

311 directly on the faunal assemblage, as shown in Fig. 2. The total studied surface covered
312 approximately 0.1 m^2.
313
314 Short-term changes were investigated for the fauna, temperature, Fe and other possible
315 explanatory variables that were deduced from images such as flux and currents. Long-term
316 variations of temperature and Fe concentrations are described in section 3.3.
317
318 **3.2.1. Environmental conditions**
319 There was a noticeable increase in temperature values and Fe concentrations between
320 P1 (4.87 ± 0.24°C, 1.02 ± 0.22 µM) and P2 (7.87 ± 1.74°C, 3.51 ± 3.08 µM), when the tip of
321 the sampling inlet was moved as described above (Figs. 4A, B). Both temperature and Fe
322 measurements recorded in the new sampling position P2 were significantly different from
323 those registered during P1 (ANOVA with permutation tests: F = 145.24, p-value = 0.001 and
324 F = 26.54, p-value = 0.001, for temperature and Fe respectively; Fig. 4). This was taken into
325 account when examining the relationships between the fauna and the environmental
326 variables; we tested the faunal changes against the environmental variables only for P1,
327 while P2 and P3 were analysed separately. The mean bottom seawater temperature in this
328 area was 4.2°C.
329
330 Vent-water flux (vertical particle velocities) and current speed (horizontal particle
331 velocities) were assessed for the entire 48-day time span (Fig. 5). They varied from 0 to 7.5
332 $cm.sec^{-1}$ for vent-water flux and from 0 to 10.5 $cm.sec^{-1}$ for current speed. They were
333 recoded into 10 classes (Table 1 for details). They were found to be negatively, but not
334 significantly, correlated with each other (Pearson correlation with permutation tests, r =

335 ¬0.2145955, p-value = 0.125). Current directions (left, right) also tended to change between
336 video recordings. However, no distinct trends were revealed.
337
338 Results of the correlogram analysis of the temperature measured on top of the mussel
339 assemblage during time interval P1 (25 days) with a resolution of one measurement per
340 hour showed a significant cyclic periodicity of ~24-25 h, corresponding to a diurnal/tidal
341 frequency (Supplementary Fig. 1). A significant negative temporal correlation was found for
342 a 12 h periodicity, corresponding to the semi-diurnal tidal periodicity (Fig. 6).
343
344 **3.2.2. Fauna**
345 **Mussels** – *Bathymodiolus azoricus*
346 Mussel abundance remained relatively constant over time in the video recordings (Fig. 6A).
347 The number of individuals ranged from 40 to 52, although most (nearly 90%) of the
348 recordings showed 45-49 mussels (Table 1). Nevertheless, the total area covered by the
349 mussels decreased slightly (-1.5%), but expanded laterally (Fig. 7). During the timespan of
350 the video recordings, one large individual died.
351
352 Overall, mussels showed a constant shell repositioning, apparently without breaking
353 their byssus threads. Only one large movement (>10 cm) by one individual was recorded. At
354 any given time, in any given recording, approximately 37% of the mussels on the still image
355 had their valves open, with a range of 16%-53%. There were no significant differences in the
356 number of open valves (log-transformed data) between the morning and evening video
357 recordings (ANOVA *F*-test: p-value = 0.384), but there were between the different
358 recordings (p-value < 0.0001). Non-significant trends of negative correlations between the

359 percentage of mussels with open valves and flux, as well as with crab abundances, were
360 observed (Pearson correlations with permutation tests, r = –0.17, p-value > 0.1 and r = –
361 0.25, p-value > 0.05 respectively).
362
363 Sudden valve closings were observed and were caused by shrimp (9.3%), limpets (0.5%)
364 or polynoids (1%) approaching siphons and edges of mussel shells, a chimaeroid passing
365 (22.3%), or crabs moving through the mussel bed (4.7%). There was no visible external
366 trigger for the remaining 62.2% of the valve closings. For all events observed, reopening
367 occurred within 10 seconds after the disturbance for 65% of the population.
368
369 **Shrimp** – *Mirocaris fortunata*
370 Shrimp abundances varied between and within video recordings, ranging from a
371 minimum abundance of 2 individuals to a maximum of 27 individuals over the entire video
372 recording period (Fig. 6B, Table 1). Shrimp abundances were positively and significantly
373 correlated with vent-water flux (Pearson correlation with permutation test, r = 0.35, p-
374 value < 0.05). There was a significant difference in shrimp abundance (log-transformed data)
375 between the morning and evening (ANOVA with permutation test, F = 7.75, p-
376 value = 0.0058), with a slightly higher abundance in the evening. There were also significant
377 differences between observation recordings (p-value < 0.0001) although the factor(s)
378 responsible for these differences remained unknown.
379
380 **Limpets –** *Pseudorimula midatlantica*
381 Abundances ranged from 0 to 8 visible individuals (Fig. 6C, Table 1). Only the individuals
382 that could be unambiguously identified as *P. midatlantica* were counted. Hence, the

abundance of this species is probably underestimated. Overall, there was an increase in *P. midatlantica* abundance over time at the beginning of the series, followed by a decrease from day 22 to day 40 and another increase towards the end. No significant links with the measured environmental variables could be established. Several individuals were seen moving around the mussel shells in the video recordings.

Crabs – *Segonzacia mesatlantica*

Abundances were low (up to 3 individuals, Fig. 6D). No links with other faunal or environmental variables could be established. Throughout the video recordings, crabs appeared to trigger valve closing in mussels when approaching them.

Polynoid polychaetes

A total of three polynoids were observed over all video recordings, probably all belonging to the species *Branchipolynoe seepensis*. Atlantic polynoid polychaete species are generally small in size (a few cm in length). Consequently, most of them were probably not visible in video stills. Therefore, these data cannot be considered representative.

Microbial mats

The percentage of the still image area covered by microbial mats increased steadily over the 48 days of the study (Fig. 6E). No significant correlation was observed between microbial mat coverage and temperature during the P1 and P2 periods (Pearson correlation with permutation tests, $r = 0.61$ and $r = 0.72$ respectively, p-values > 0.2). Moreover, there was no significant correlation between faunal abundance and microbial coverage.

3.3. Long-term changes in faunal distribution between 2006 and 2008

The surface area covered by the wide-angle photographs was 0.99 m^2 in 2006 and 0.87 m^2 in 2008. Our image analysis showed that there was an 11% increase in mussel coverage and a 4% increase in microbial coverage between 2006 and 2008 (Table 2). The densities of the mussels also increased by ~140 $ind.m^{-2}$. Conversely, for shrimps and crabs, there was a decrease in densities from 42.3 $ind.m^{-2}$ to 30.9 $ind.m^{-2}$ for *M. fortunata* and from 6 $ind.m^{-2}$ to 3.4 $ind.m^{-2}$ for *S. mesatlantica*.

The delineated surface area of the close-up photographs (Fig. 7) was approximately the same (~0.1 m^2) for 2006 and 2008. Similar to what was observed in the wide-angle photographs, image analysis showed an increase (~12%) in mussel coverage along with an increase in mussel densities between the two years (Table 2). However, the increase in microbial coverage observed in the wide-angle photographs was not detectable when analysing the close-up photographs (Fig. 7). Rather, there was a very slight decrease in microbial cover (~0.14%; Table 2) and mussels seemed to have replaced the microbial mats in certain areas (Fig. 7). The decrease in shrimp and crabs, described above (section 3.2.2), was also observed in the close-up photographs with a decrease of 145.4 $ind.m^{-2}$ for the former and 19.9 $ind.m^{-2}$ for the latter.

3.4. Long-term changes in environmental variables

3.4.1. Temperature

Over the period of nearly one year of data analysed (P3), temperature values varied between 4.02°C and 18.33°C for a mean of 7.20 ± 1.6°C (Fig. 4A). 46.5% (3977) recorded temperatures between 4.20 and 6.99°C followed by 47.2% (4036) in the 7.00-9.99°C range;

6% (517) were recorded between 10.00 and 13.90°C and only 0.2% (18) were over 14°C. No significant linear trend was detected, but variations in temperature values were observed with several incursions over 10°C (Fig. 4A).

Whittaker-Robinson periodogram analyses were carried out on the 8548 hourly temperature values (P3), allowing a first preliminary assessment and a selection of possible periods of interest. Subsequently, various periodograms from periods of 1 to 50 h, 1 week, 1 month, 3 months and finally almost 6 months were calculated. The main significant periods in temperature variation found within a two-month time span are shown in Fig. 8. These periods accounted for significant harmonics found at higher frequencies. The first significant values were for the 12 h and 24 h periods (Fig. 8). Additional significant periods were found between periods T = 634 h and 708 h, which correspond to between 26.4 and 29.5 days. A more pronounced grouping of significant periods in temperature variation was found between T = 1265 h and 1392 h, or 52.7 to 58 days. Several harmonics of basic periods (e.g. semi-diurnal and diurnal) are visible within this two-month period, while some harmonics of low-frequency periods (e.g. lunar cycle) were found in the periodograms spanning 3 months and 6 months (not shown).

3.4.2. Iron concentrations (Fe)

The entire Fe data set contained 259 measurements representing 133 days with measurements taken every 12 h (Fig. 4B). The mean Fe concentration was 3.2 ± 2.4 µM with a maximum value of 16.5 µM and a minimum value of 0.62 µM (close to the detection limit). No significant linear trends were detected but a few incursions over 5 µM were observed. The periodogram was constructed for 117 days of measurements (P2 and P3). Significant

455 periods were found around 30 days (T = 60), which may correspond to the lunar cycle. One
456 significant harmonic value was found at 55.5 days (Fig. 9).
457
458 **4. Discussion**
459 The TEMPO observatory experiment described in this study lasted nearly 2 years, with
460 different levels of data acquisition. To our knowledge, the analysis presented here is one of
461 the longest integrated (faunal and environmental data) time series obtained to date in a
462 hydrothermal ecosystem. It provides the first insights on day-to-day variations in a
463 *Bathymodiolus azoricus* mussel assemblage. Additional observations supply valuable
464 information on longer-term variations in temperature and Fe concentrations, although
465 these were not coupled with image data. The methodological approach developed for this
466 experiment can serve as an example to determine what kind of information can be
467 extracted from deep-sea observatories, and to explore the links between variables acquired
468 at different spatial and temporal scales.
469
470 **4.1 Short-term changes**
471 The significant increase in measured environmental factors between the first (P1) and
472 second (P2) periods of the video recording was due to a slight displacement of the water
473 sampling inlet by a chimaeroid fish. This increase illustrates the high heterogeneity within
474 habitats in the vent ecosystem, even at the scale of a few centimetres (Sarrazin et al., 1999;
475 Cuvelier et al., 2009). Temperature readings (mean 4.87 ± 0.24°C) along with iron
476 concentrations (mean 1.02 ± 0.22µM) measured on the mussel assemblage (P1) were
477 representative of a very limited input of hydrothermal fluids. The temperature variations
478 are in the same range as those observed by Khripounoff et al., (2008) 10 m above the

seafloor in the LS vent field, outside the vent influence. They are also similar to the lower end of the temperatures measured in *Bathymodiolus azoricus* microhabitats on Eiffel Tower (De Busserolles et al., 2009; Cuvelier et al., 2009).

Patterns in temperature variation — Over the 25-day period (P1), the temperature time series showed a ~24-25 h cyclic periodicity and a negative temporal autocorrelation at 12 h. These values correspond to the tidal signal observed in the LS vent field at 25 h and to the semi-diurnal tidal oscillation at 12.30 h (Khripounoff et al., 2000, 2008). They are also concordant with bottom pressure data acquired in the same area and for which significant periodicities matched the tidal signal and its harmonics (periodogram not shown; V. Ballu, unpublished data). For comparison, a 12.4 h periodicity in vent temperature time-series records has also been observed on the Juan de Fuca Ridge (Pacific Ocean), along with a 16-17 h inertial peak and a broadband peak centred at 4–5 days (Tivey et al. 2002). Variability in bottom temperatures and currents at LS also appear to be influenced, but to a lesser extent, by inertial oscillations (at about 20 h, Khripounoff et al., 2008). Evidence for modulation of diffuse flow by tides has been provided by several temperature time-series measurements at hydrothermal vents (review by Tivey et al., 2002; Scheirer et al., 2006).

The potential mechanisms causing this tide-related variability include the modulation of seafloor and hydrostatic pressure fields by ocean tides, modulation of horizontal bottom currents by tides and solid Earth tide deformations (Schultz and Elderfield, 1997; Davis and Becker, 1999). While time-series records from low-temperature diffuse flow emissions indicate modulation of temperature by tidally induced changes in bottom currents (Little et al., 1988), high-temperature, high-flow vents (smokers) do not exhibit this tidal variability

503 (Fornari et al., 1998; Tivey et al., 2002), suggesting that areas of higher fluid flow are less
504 influenced by tides or that stronger flow variations may mask the tidal signal.
505
506 *Links between faunal distribution and environmental conditions* — Tidal cycles may have
507 an impact on vent communities by modifying the degree of mixing of hydrothermal fluids
508 with seawater, particularly in the near-bottom benthic boundary layer (BBL). Vent
509 communities found at the BBL may be modified by rapid changes in tidal current direction
510 and speed, inducing variation in temperature and related environmental conditions
511 (Sarradin et al., 2009). Therefore, as the current speed varies between flood and ebb tides,
512 the BBL shifts from a situation where the diffuse vent fluids are swept laterally along the
513 seafloor towards one where plumes rise as a result of their buoyancy (Hautala et al., 2012).
514 Visual observations of particle movements in our video images support this hypothesis: the
515 particles flowed laterally when the tidal current dominated and rose when the
516 hydrothermal flux prevailed. Semi-diurnal variations of water flow and diurnal fluctuations
517 of suspended particle loads have also been reported during a 6 day deployment on the Juan
518 de Fuca Ridge (Johnson and Tunnicliffe 1985). Although not observed in our data, temporal
519 variation in hydrodynamic processes may influence the availability of oxygen, chemicals and
520 food resources for the fauna and can have significant effects on biological communities
521 (Sarrazin et al., 1999; De Busserolles et al., 2009).
522
523 Little information and data on the effects of “moderate” environmental variation on the
524 hydrothermal fauna are available for vent ecosystems. Several studies suggested that there
525 is a strong link between faunal distribution, population dynamics and hydrothermal
526 environmental conditions (Sarrazin et al., 1999, 2006, Govenar and Fisher 2007, Cuvelier et

527 al., 2009, Ivanenko et al., 2012, Sen et al., 2013), supporting the idea that the fauna respond
528 quickly to "abiotically challenging" environments (Girguis and Lee, 2006). Modifications in
529 fluid flow may influence resource availability (De Busserolles et al., 2009, Beinart et al.,
530 2012) by inducing changes in microbial production (Guezenec et al., 1998; Sievert et al.,
531 2000) and/or the abundance of symbionts (Halary et al., 2008; Robidart et al., 2011).
532 Changes in fluid flow may also influence metal bioavailability (Cosson et al., 2008; Sarradin
533 et al., 2009) and radionuclide exposure (Charmasson et al., 2009). Therefore, even
534 moderate changes in hydrothermal habitats are expected to lead to a rapid response of the
535 hydrothermal fauna, driven by their individual needs and tolerance.
536
537 In our study, the abundances of *Bathymodiolus azoricus* mussels and *Segonzacia*
538 *mesatlantica* crabs were quite stable over time, reflecting the relative stability of
539 environmental conditions during the 48-day video monitoring period. The abundances of
540 *Mirocaris fortunata* shrimp varied with time and were significantly correlated with
541 variations in hydrothermal fluid flow. A video camera deployed on the Trans-Atlantic
542 Geotraverse (TAG) hydrothermal edifice (on the MAR) recorded an increase in shrimp
543 densities, concordant with a local increase in temperature (Copley et al., 1999). The positive
544 relationship of this species with the intensity of hydrothermal emissions (and temperature)
545 is consistent with its distribution in the vicinity of active diffusers, in thermal conditions
546 ranging from 2 to 25°C (Segonzac et al., 1992; Gebruk et al., 1997; Polz et al., 1998; Van
547 Dover et al., 1996; Desbruyères et al., 2001; Copley et al., 2007). Spatial distribution of *M.*
548 *fortunata* shrimp can be explained by their nutritional requirements as they may feed on
549 species relying on free-living bacteria (Segonzac et al., 1993; Gebruk et al., 2000; Colaço et

550 al., 2002). Their high $\delta^{15}N$ values support the hypothesis that they may be predators of
551 bacterivorous and scavenger species (De Busserolles et al., 2009).
552
553 As in the case of most of the studied species, the abundance of *Pseudorimula*
554 *midatlantica* limpets varied through time, but no links could be established with
555 environmental conditions. Similarly, no correlation between the abundance of buccinid
556 gastropods and fluid temperature was observed on the Juan de Fuca Ridge (Martell et al.,
557 2002). A significant increase in microbial cover was noticeable from day 10 to the end of the
558 video recording period. A link with variation in hydrothermal fluid inputs was suspected, but
559 this hypothesis was not statistically supported. Finally, although no significant influence of
560 the tides was observed on the fauna, it is likely that physiological processes and species
561 activities are influenced by these periodic variations. Longer time series, coupling video
562 recordings and environmental data, are needed to test this hypothesis. Other physical and
563 chemical data (current measurements as well as oxygen, sulphide and methane
564 concentrations) would be useful additions to time-series analyses.
565
566 *Role of catastrophic events* — With the exception of the chimaeroid passage, which
567 affected our data recording, no catastrophic event was observed during the 48-day period.
568 Chimney collapses and landslides are frequent in the hydrothermal environment and can
569 have significant destructive impacts on faunal communities (Johnson and Tunnicliffe, 1988;
570 Tunnicliffe, 1991; Sarrazin et al., 1997). Our most recent TEMPO time series (2011) captured
571 the growth of a small 4 cm chimney, but no immediate or visible effect was noticeable on
572 the surrounding fauna (Sarrazin et al., unpublished data). Conversely, one of the rare
573 continuous video records in the vent environment (26 days in 1986) filmed the growth and

574 collapse of small anhydrite chimneys that caused the death of about 44% of the *Ridgeia*
575 *piscesae* tubeworm (siboglinid polychaetes) community on the Axial volcano (northern East
576 Pacific Rise; Tunnicliffe and Juniper, 1990). Mid-ocean ridge volcanic activity can also have
577 significant effects on hydrothermal emissions, not only affecting areas of diffuse venting but
578 also microbial coverage, as observed in 2001 during a major magmatic dike intrusion on LS
579 (Dziak et al., 2004). Even though seismic activity is continuously recorded in the LS region
580 through the MoMAR observatory (Cannat et al., unpublished data), its magnitude over the
581 past decade appear to be too low to cause visible impacts on the geological structures and,
582 consequently, on the mussel communities at large scales (Cuvelier et al., 2011b).
583
584 **4.2 Long-term changes**
585 *Environmental conditions* – During this study, temperature varied between ~4 and
586 16.9°C in the study area. Significant periodicities in temperature were found, closely
587 corresponding to the tidal (diurnal 24 h 50 min and semi-diurnal 12 h 25 min), lunar (a lunar
588 month is about 29.53 days) and two lunar (52.7-58 days) cycles. Several harmonics of basic
589 and low-frequency periods were also found in the longer periodograms. For Fe
590 concentrations, only periodicities linked to the lunar cycle (30 and 55.5 days) were found.
591 Longer time series as well as higher-frequency measurements, will be necessary to pinpoint
592 significant periods.
593
594 *Faunal changes* — No drastic faunal changes occurred between the two years of the study.
595 A slight increase in mussel and microbial coverage was observed between 2006 and 2008.
596 Mussel densities also increased while those of shrimp and crabs decreased. With the
597 exception of microbial coverage, similar patterns were observed in the close-up and wide-

598 angle images, suggesting that the results obtained by a camera with a limited "observation"
599 surface can be supplemented with observations at broader spatial scale. Individual growth
600 rates could not be estimated, although this information would have been useful to better
601 understand their relationships with variation in environmental conditions. Two recent
602 studies have shown that *Bathymodiolus* growth rates exhibit tide-related variability (Schöne
603 and Giere, 2005; Nedoncelle et al., 2013), possibly reflecting the variability of the mixing
604 ratio between hydrothermal fluids and sea water and subsequently their influence on
605 energy resources for symbionts (Nedoncelle et al., 2013). The addition of a laser grid on the
606 camera could help us estimate growth dynamics from video images, although it would be a
607 challenge to distinguish individuals without marking them.
608
609 **4.3 Behavioural observations**
610 To date, only a few studies have addressed behavioural issues in response to short-term
611 variation in hydrothermal conditions in vent ecosystems (Tunnicliffe et al., 1990, Grelon et
612 al., 2006) and only rare observations of species interactions are available. Clearly,
613 continuous video monitoring associated with environmental sensing is a promising avenue
614 of research to collect quantitative information on rates of change, biological rhythms and
615 species interactions in these remote ecosystems. *Bathymodiolus azoricus* mussels show
616 constant shell repositioning, but only one individual moved as far as 10 cm from its original
617 position. At all times, about 37% of the mussels had their valves open, but no link with
618 environmental conditions or the presence of other fauna could be established yet. Some
619 mussels were observed reacting to the surrounding fauna by closing their valves when a
620 contact was made. This immediate response to tactile stimuli, also observed in vent
621 tubeworms (Tunnicliffe et al., 1990), suggests a protective mechanism against predators.

622

623 The *Mirocaris fortunata* shrimp were very active on the substrate. They appeared to be
624 particularly attracted to the presence of diffuse venting and their densities varied with
625 respect to changes in fluid flow. As suggested above, their higher occurrence in areas of
626 stronger fluid emission may be linked to the presence of increased food sources. For
627 example, Sievert et al. (2000) showed an increase in the abundance of microorganisms
628 along a thermal gradient, indicating that microbial activity is stimulated by high
629 temperatures and vent fluid flow. Similarly, Guezennec et al. (1998) observed a clear
630 influence of fluid flow intensity on the development of biofilms at vents.

631

632 Very few direct interactions were observed between the vent species studied here,
633 although aggressive behaviour was sporadically observed between crabs and shrimp. On a
634 few occasions, the crabs chased the shrimp by moving towards them and displaying their
635 claws, but these movements did not result in catching shrimp, suggesting that this
636 behaviour was more territorial than predatory. Finally, although not significant, there was a
637 negative correlation between the presence of vent gastropods and microbial coverage. We
638 suggest that this may reflect grazing activity, with areas of abundant gastropod densities
639 being cleaned of bacterial mats (De Busserolles et al. 2009). The acquisition of longer faunal
640 time series will bring more insight into specific aspects of species behaviour, possibly leading
641 to a better understanding of other important biological factors, such as growth and
642 mortality.

643

644 **5. Conclusions**

645 Hydrothermal faunal assemblages at the LS vent field on the MAR are far more stable
646 than anticipated and the relative steadiness of environmental factors was a surprise in an
647 ecosystem characterised by extreme abiotic conditions. A key finding of this study is that the
648 vent fauna of the filmed assemblage appear to be present in quite stable microhabitats,
649 characterised by low hydrothermal inputs, where temperatures rarely exceed 20°C.
650
651 The major limitation of our study arises from the fact that our analysis is based on a
652 single faunal assemblage with only a few environmental measurements taken at small
653 spatial scale, which is obviously not sufficient to describe the complexity of hydrothermal
654 ecosystems. Although the observations made via a single deep-sea observatory are limited
655 in spatial extent, they bring fundamental ecological insights into the dynamics of vent
656 communities to which we did not have access previously. As shown by our long-term
657 results, extrapolated from photographs taken in 2006 and 2008, these spatially-limited
658 temporal observations may be supplemented with broader-scale video images repeatedly
659 acquired by submersibles.
660
661 Recommendations for future work include the increase in spatial resolution of
662 continuous temperature measurements (used as a proxy for hydrothermal inputs), which
663 are essential to capture the small-scale heterogeneity of the habitat (2- or 3D mapping,
664 Rinke and Lee 2009). The acquisition of video data should be performed in triplicate (i.e.
665 three cameras on three assemblages) and complemented by periodic ROV video transects at
666 the edifice scale. Temporal studies should be designed to address a specific aspect of
667 species behaviour, with the acquisition of higher-frequency data and continuous monitoring
668 of key environmental factors. Finally, as all organisms are not visible on the image, the fauna

associated with an assemblage similar to the filmed assemblage should be sampled and its habitat characterised to supplement the data acquired by the observatory, providing an accurate portrait of the biodiversity.

In the near future, assessment of the effects of larger-scale environmental factors (such as seismicity, seafloor deformation, chemical variations, currents) on local environmental conditions as well as on the structure of vent communities is planned, using the integrated data sets acquired through the MoMAR deep-sea observatory deployed since 2010 (Cannat et al., 2011).

6. Acknowledgements

The captains and crews of the R/Vs *Pourquoi pas?* and *L'Atalante* and the pilots of the ROV *Victor6000* are warmly acknowledged for their dedicated assistance and for contributing to the success of the MoMARETO and MoMAR08 cruises. The chief scientists of these cruises were Jozée Sarrazin and Pierre-Marie Sarradin for MoMARETO (2006) and Javier Escartin for MoMAR08 (2008). The TEMPO module was designed and built during the EXOCET/D EU project (GOCE505342) and we thank the engineers who were involved in the conception of this first version: Jérôme Blandin, Laurent Delauney, Stéphane Dentrecolas, Philippe Dorval, Jacky Dupont, Julien Legrand, Christian Le Gall, Dominique Le Roux, Michel Hamon, Jean-Pierre Sudreau, Pierre Léon, Jean-Pierre Lévèque, Philippe Rodier, Renaud Vuillemin. We also acknowledge Valérie Ballu (CNRS/Université de La Rochelle) who kindly provided us with her pressure data from the MAR, the LEP instrumentation team who is indispensable on land and at sea and Julie Tourolle for her help with the maps. This research project was funded by a grant from the national research agency (*Agence Nationale de la Recherche*,

693 ANR DEEP-OASES (ANR06BDV005)) and supported by the Research Federation (GDR)
694 ECCHIS. This manuscript was professionally edited by Carolyn Engel-Gautier. Thanks to the
695 three anonymous reviewers for their thorough reviews and comments which improved the
696 manuscript and to associate editor Andy Gooday for his help in guiding and editing the
697 manuscript.

698

699 **7. References**

700 Barreyre T, Escartín J, Garcia R, Cannat M, Mittelstaedt E, Prados R (2012). Structure,
701 temporal evolution, and heat flux estimates from the Lucky Strike deep-sea hydrothermal
702 field derived from seafloor image mosaics. Geochemistry, Geophysics, Geosystems
703 13:Q04007; doi: 10.1029/2011GC003990.

704

705 Beinart RA, Sanders JG, Faure B, Sylva SP, Lee RW, Becker E, Gartman A, Luther GW III,
706 Seewald JS, Fisher CR, Girguis PR (2012). Evidence for the role of endosymbionts in regional-
707 scale habitat partitioning by hydrothermal vent symbioses. Proceedings of the National
708 Academy of Sciences of the United States of America 109:E3241–E3250;
709 doi:10.1073/pnas.1202690109.

710

711 Blandin J, Rolin JF (2005). An array of sensors for the seabed monitoring of geohazards, a
712 versatile solution for the long-term real-time monitoring of distributed seabed parameters.
713 Sea Technology, 46:33–36.

714

715 Cannat M, Sarradin PM, Blandin J, Escartin J, Colaco A, the MoMAR-Demo Scientific Party
716 (2011). MoMar-Demo at Lucky Strike. A near-real time multidisciplinary observatory of
717 hydrothermal processes and ecosystems at the Mid-Atlantic Ridge. Abstract OS22A-05
718 presented at 2011 Fall Meeting, AGU, San Francisco, Calif., 5-9 Dec.

719

720 Charlou JL, Donval JP, Douville E, Jean-Baptiste P, Radford-Knoery J, Fouquet Y, Dapoigny A,
721 Stievenard M (2000). Compared geochemical signatures and the evolution of Menez Gwen
722 (37°50'N) and Lucky Strike (37°17'N) hydrothermal fluids, south of the Azores Triple Junction

723 on the Mid-Atlantic Ridge. Chemical Geology 171:49-75; doi:10.1016/S0009-2541(00)00244-
724 8.

725

726 Charmasson S, Sarradin PM, Le Faouder A, Agarande M, Loyen J, Desbruyères D (2009). High
727 levels of natural radioactivity in biota from deep-sea hydrothermal vents: a preliminary
728 communication. Journal of Environmental Radioactivity 100:522–526;
729 doi:10.1016/j.jenvrad.2009.02.002.

730

731 Colaço A, Dehairs F, Desbruyères D, Le Bris N, Sarradin PM (2002). $\delta^{13}C$ signature of
732 hydrothermal mussels is related with the end-member fluid concentrations of H_2S and CH_4
733 at the Mid-Atlantic Ridge hydrothermal vent fields. Cahiers de Biologie Marine 43:259-262.

734

735 Colaço A, Blandin J, Cannat M, Carval T, Chavagnac V, Connelly D, Fabian M, Ghiron S, Goslin
736 J, Miranda JM, Reverdin G, Sarrazin J, Waldmann C, Sarradin PM (2011) MoMAR-D: a
737 technological challenge to monitor the dynamics of the Lucky Strike vent ecosystem. ICES
738 Journal of Marine Science 68:416-424; doi: 10.1093/icesjms/fsq075.

739

740 Copley JTP, Tyler PA, Murton BJ, Van Dover CL (1997). Spatial and interannual variation in
741 the faunal distribution at Broken Spur vent field (29°N, Mid-Atlantic Ridge). Marine Biology
742 129: 723-733.

743

744 Copley JTP, Tyler PA, Murton BJ, Van Dover CL (1999). Spatial and interannual variation in
745 the faunal distribution at Broken Spur vent field (29°N, Mid-Atlantic Ridge). Marine Biology
746 129:723-733.

Copley JTP, Jorgensen PBK, Sohn RA (2007). Assessment of decadal- scale ecological change at a deep Mid-Atlantic hydrothermal vent and reproductive time-series in the shrimp *Rimicaris exoculata*. Journal of the Marine Biological Association of the United Kingdom 84:859-867; doi:10.1017/S0025315407056512.

Cosson RP, Thiébaut E, Company R, Castre-Rouelle M, Colaço A, Martins I, Sarradin PM, Bebianno MJ (2008) Spatial variation of metal bioaccumulation in the hydrothermal vent mussel *Bathymodiolus azoricus*. Marine Environmental Research 65:405-415; doi:0.1016/j.marenvres.2008.01.005.

Cuvelier D, Sarrazin J, Colaço A, Copley J, Desbruyères D, Glover AG, Tyler P, Serrão Santos R (2009). Distribution and spatial variation of hydrothermal faunal assemblages at Lucky Strike (Mid-Atlantic Ridge) revealed by high-resolution video image analysis. Deep-Sea Research I 56:2026–2040; doi:10.1016/j.dsr.2009.06.006.

Cuvelier D, Sarradin PM, Sarrazin J, Colaço A, Copley JT, Desbruyères D, Glover AG, Serrão Santos R, Tyler PA (2011a). Hydrothermal faunal assemblages and habitat characterisation at the Eiffel Tower edifice (Lucky Strike, Mid-Atlantic Ridge). Marine Ecology 32:243-255; doi:10.1111/j.1439-0485.2010.00431.x.

Cuvelier D, Sarrazin J, Colaço A, Copley JT, Glover AG, Tyler PA, Serrão Santos R, Desbruyères D (2011b). Community dynamics over 14 years at the Eiffel Tower hydrothermal edifice on

the Mid-Atlantic Ridge. Limnology and Oceanography 56:1624-1640; doi:10.4319/lo.2011.56.5.1624.

Cuvelier D, De Busserolles F, Lavaud R, Floc'h E, Fabri MC, Sarradin PM, Sarrazin J (2012). Biological data extraction from imagery – How far can we go? A case study from the Mid-Atlantic Ridge. Marine Environmental Research 82:15-27; doi:10.1016/j.marenvres.2012.09.001.

Cuvelier D, Beesau J, Viatcheslav NI, Zeppilli D, Sarradin PM, Sarrazin J (2014). First insights into macro- and meiofaunal colonisation patterns on paired wood/slate substrata at Atlantic deep-sea hydrothermal vents. Deep Sea Research I 87: 70-81.

Davis E, Becker K (1999). Tidal pumping of fluids within and from the oceanic crust: new observations and opportunities for sampling the crustal hydrosphere. Earth and Planetary Science Letters 172:141-149; .doi:10.1016/S0012-821X(99)00197-1.

De Busserolles F, Sarrazin J, Gauthier O, Gélinas Y, Fabri MC, Sarradin PM, Desbruyères D (2009). Are spatial variations in the diets of hydrothermal fauna linked to local environmental conditions? Deep-Sea Research II 56:1649-1664; doi: 10.1016/j.dsr2.2009.05.011.

Desbruyères D, Almeida A, Biscoito M, Comtet T, Khripounoff A, Le Bris N, Sarradin PM, Segonzac M (2000). A review of the distribution of hydrothermal vent communities along

the Northern Mid-Atlantic Ridge: Dispersal vs environmental controls. Hydrobiologia 440:201-216.

Desbruyères D, Biscoito M, Caprais JC, Colaço A, Comtet T, Crassous P, Fouquet Y, Khripounoff A, Le Bris N, Olu K, Riso R, Sarradin PM, Segonzac M, Vangriesheim A (2001). Variations in deep-sea hydrothermal vent communities on the Mid-Atlantic Ridge when approaching the Azores Plateau. Deep-Sea Research I 48:1325-1346.

Dziak RP, Smith DK, Bohnenstiehl DR, Fox CG, Desbruyères D, Matsumoto H, Tolstoy M, Fornari DJ (2004). Evidence of a recent magma dike intrusion at the slow spreading Lucky Strike segment, Mid-Atlantic Ridge. Journal of Geophysical Research-Solid Earth 109:B12102; doi:10.1029/2004JB003141.

Fisher CR, Childress JJ, Arp AJ, Brooks JM, Distel D et al. (1988). Microhabitat variation in the hydrothermal vent mussel Bathymodiolus thermophiles at the Rose Garden vent on the Galapagos rift. Deep Sea Research I 35: 1769-1791.

Fornari DJ, Shank T, Von Damm KL, Gregg TKP, Lilley M, Levai G, Bray A, Haymone RM, Perfit MR, Lutz R (1998). Time-series temperature measurements at high-temperature hydrothermal vents, East Pacific Rise 9°49 –51 N: evidence for monitoring a crustal cracking front. Earth and Planetary Science Letters 160:419–431; doi:10.1016/S0012-821X(98)00101-0.

816 Fouquet Y, Ondreas H, Charlou JL, Donval JP, Radfordknoery J, Costa I, Lourenco N, Tivey MK
817 (1995). Atlantic lava lakes and hot vents. Nature 377:201-201; doi:10.1038/377201a0.
818
819 Gebruk AV, Galkin SV, Vereshchaka AL, Moskalev LI, Southward AJ (1997). Ecology and
820 biogeography of the hydrothermal vent fauna of the Mid-Atlantic Ridge. Advances in Marine
821 Biology 32:93-144; doi:10.1016/S0065-2881(08)60016-4.
822
823 Gebruk AV, Southward EC, Kennedy H, Southward AJ (2000). Food sources, behaviour, and
824 distribution of hydrothermal vent shrimps at the Mid-Atlantic Ridge. Journal of the Marine
825 Biological Association of UK 80:485-499.
826
827 Gebruk A, Fabri MC, Briand P, Desbruyères D (2010). Community dynamics over a decadal
828 scale at Logatchev, 14°45'N Mid-Atlantic Ridge. Cahiers de Biologie Marine 51: 383-388.
829
830 Girguis PR, Lee R. (2006). Thermal preference and tolerance of Alvinellids. Nature 312:231.
831
832 Guezennec J, Ortega-Morales O, Raguenes G, Geesey G (1998). Bacterial colonization of
833 artificial substrate in the vicinity of deep-sea hydrothermal vents. FEMS Microbiology
834 Ecology 26: 89-99; doi: 10.1111/j.1574-6941.1998.tb00495.x.
835
836 Glover AG, Gooday AJ, Bailey DM, Billett DSM, Chevaldonné P, Colaço A, Copley J, Cuvelier
837 D, Desbruyères D, Kalogeropoulou V, Klages M, Lampadariou N, Lejeusne, C, Mestre NC,
838 Paterson GLJ, Perez T, Ruhl H, Sarrazin J, Soltwedel T, Soto EH, Thatje S, Tselepides A, van
839 Gaever S, Vanreusel A (2010). Temporal change in deep-sea benthic ecosystems: a review of

the evidence from recent time-series studies. Advances in Marine Biology 58:1-95; doi:10.1016/B978-0-12-381015-1.00001-0.

Govenar B, Fisher CR (2007). Experimental evidence of habitat provision by aggregations of *Riftia pachyptila* at hydrothermal vents on the East Pacific Rise. Marine Ecology 28: 3-14.

Grelon D, Morineaux M, Desrosiers G, Juniper SK (2006). Feeding and territorial behavior of *Paralvinella sulfincola*, a polychaete worm at deep-sea hydrothermal vents of the Northeast Pacific Ocean, Journal of Experimental Marine Biology and Ecology 329: 174-186.

Guezennec J,Ortega-Morales O, Raguenes G, Geesey G (1998).Bacterial colonization of artificial substrate in the vicinity of deep-sea hydrothermal vents. FEMSMicrobiologyEcology 26: 89-99.

Halary S, Riou V, Gaill F, Boudier T, Duperron S (2008). 3D FISH for the quantification of methane- and sulphur-oxidising endosymbionts in bacteriocytes of the hydrothermal vent mussel *Bathymodiolus azoricus*. The ISME Journal 2:284-292; doi:10.1038/ismej.2008.

Hautala S, Johnson HP, Pruis M, García-Berdeal I, Bjorklund T (2012). Low-temperature hydrothermal plumes in the near-bottom boundary layer at Endeavour Segment, Juan de Fuca Ridge. Oceanography 25:192–195; doi:10.5670/oceanog.2012.17#sthash.a15cB3Dv.dpuf.

863 Ivanenko VN, Corgosinho PHC, Ferrari FD, Sarradin PM, Sarrazin J (2012). Microhabitat
864 distribution of *Smacigastes micheli* (Copepoda: Harpacticoida: Tegastidae) from deep-sea
865 hydrothermal vents at the Mid-Atlantic Ridge, 37°N (Lucky Strike), with a morphological
866 description of the nauplius. Marine Ecology 3:245-256; doi: 10.1111/j.1439-
867 0485.2011.00484.x.
868
869 Johnson HP, Tunnicliffe V (1985). Time-series measurements of hydrothermal activity on
870 northern Juan de Fuca Ridge. Geophysisal Research Letters 12: 685-688.
871
872 Johnson HP, Tunnicliffe V (1988). Time-lapse photography of a hydrothermal system: a
873 successful one-year deployment. EOS 9: 1024-1026.
874
875 Khripounoff A, Comtet T, Vangriesheim A, Crassous P (2000). Near-bottom biological and
876 mineral particle flux in the Lucky Strike hydrothermal vent area (Mid-Atlantic Ridge). Journal
877 of Marine Systems 25:101-118; doi:10.1016/S0924-7963(00)00004-X.
878
879 Khripounoff A, Vangriesheim A, Crassous P, Segonzac M, Lafon V, Waren A (2008). Temporal
880 variation of currents, particulate flux and organism supply at two deep-sea hydrothermal
881 fields of the Azores Triple Junction. Deep-Sea Research I 55:532-551;
882 doi:10.1016/j.dsr.2008.01.001.
883
884 Legendre P (2012) WR periodogram. R function available on the Web page
885 numericalecology.com.
886

887 Legendre P, Legendre L (2012) Numerical ecology. Third English Edition. Elsevier Science BV.

888

889 Little SA, Stolzenbach KD, Grassle FJ (1988). Tidal current effects on temperature in diffuse
890 hydrothermal flow: Guaymas Basin. Geophysical Research Letters 15:1491-1494;
891 doi:10.1029/GL015i013p01491.

892

893 Luther GW, Rozan TF, Taillefert M, Nuzzio DB, Di meo C, Shank T, Lutz R, Cary C (2001).
894 Nature 410: 813-816.

895

896 Marcus J, Tunnicliffe V, Butterfield D (2009). Post-eruption succession of macrofaunal
897 communities at diffuse flow hydrothermal vents on Axial Volcano, Juan de Fuca Ridge,
898 northeast Pacific. Deep-Sea Research II: 56:1586-1598; doi: 10.1016/j.dsr2.2009.05.004.

899

900 Marsh L, Copley JT, Huvenne VAI, Linse K, Reid WDK, Rogers AD, Sweeting CJ, Tyler PA
901 (2012). Microdistribution of Faunal Assemblages at Deep-Sea Hydrothermal Vents in the
902 Southern Ocean. PLoS ONE 7(10): e48348. doi:10.1371/journal.pone.0048348.

903

904 Martell KA, Tunnicliffe V, MacDonald IR (2002). Behaviour and population features of a
905 buccinid whelk (Gastropoda, Neogastropoda) at the Endeavour Vent fields of Juan de Fuca
906 Ridge, Northeast Pacific. Journal of Molluscan Studies 68: 45-53.

907

908 Nedoncelle K, Lartaud F, de Rafelis M, Boulila S, Le Bris N (2013). A new method for high-
909 resolution bivalve growth rate studies in hydrothermal environments. Marine Biology 160:
910 1427-1439.

Nees HS, Moore TS, Mullaugh KM, Holyoke RR, Janzen CP, Ma S, Metzger E, Waite TJ, Yücel M, Lutz RA, Shank TM, Vetriani C, Nuzzio DB, Luther GW III (2008). Hydrothermal vent mussel habitat chemistry, pre- and post-eruption at 9°50 North on the East Pacific Rise. Journal of Shellfish Research 27:169-175; doi:10.2983/0730-8000.

Nye V, Copley JT, Tyler PA (2013). Spatial Variation in the Population Structure and Reproductive Biology of Rimicaris hybisae (Caridea: Alvinocarididae) at Hydrothermal Vents on the Mid-Cayman Spreading Centre. PLoS ONE 8(3): e60319. doi:10.1371/journal.pone.0060319.

Ondréas H, Cannat M, Fouquet Y, Normand A, Sarradin PM, Sarrazin J (2009). Recent volcanic events and the distribution of hydrothermal venting at the Lucky Strike hydrothermal field, Mid-Atlantic Ridge. Geochemistry Geophysics Geosystems 10:Q0AG14; doi:10.1029/2008GC002171.

Podowski EL, Moore TS, Zelnio KA, Luther GW III, Fisher CR (2009). GIS-based analysis of realized distributional patterns of diffuse flow megafauna on the Eastern Lau Spreading Center, Tonga. Deep-Sea Research I 56:2041-2056.

Polz MF, Robinson JJ, Cavanaugh CM, Van Dover CL (1998). Trophic ecology of massive shrimp aggregations at a Mid-Atlantic Ridge hydrothermal vent site. Limnology and Oceanography 43:1631-1638.

935 Rasband WS (2012). ImageJ, U.S. National Institutes of Health, Bethesda, Maryland, USA,
936 http://imagej.nih.gov/ij/, 1997-2012.
937
938 R Development Core Team (2012). R: A language and environment for statistical computing.
939 R Foundation for Statistical Computing, Vienna, Austria. ISBN 3-900051-07-0. http://www.R-
940 project.org/.
941
942 Rinke C, Lee RW (2009). Macro camera temperature logger array for deep-sea hydrothermal
943 vent and benthic studies. Limnology and Oceanography 7: 527-534.
944
945 Robidart JC, Roque A, Song P, Girguis PR (2011). Linking hydrothermal geochemistry to
946 organismal physiology: physiological versatility in *Riftia pachyptila* from sedimented and
947 basalt-hosted vents. PLoS ONE 6:e21692; doi:10.1371/journal.pone.0021692
948
949 Santos RS, Colaço A, Christiansen S. (eds) (2003). Planning the management of deep-sea
950 hydrothermal vent fields MPA in the Azores Triple Junction (Proceedings of the workshop).
951 Arquipélago. Life and Marine Sciences. Supplement 4: xii + 70 pp.
952
953 Sarradin PM, Waeles M, Bernagout S, Le Gall C, Sarrazin J, Riso R (2009). Speciation of
954 dissolved copper within an active hydrothermal edifice on the Lucky Strike vent field (MAR,
955 37°N). Science of the Total Environment 407:869-878.
956

957 Sarrazin J, Robigou V, Juniper SK, Delaney JR (1997). Biological and geological dynamics over
958 four years on a high-temperature sulphide structure at the Juan de Fuca Ridge hydrothermal
959 observatory. Marine Ecology Progress Series 153:5-24; doi:10.3354/meps153005.
960
961 Sarrazin J, Juniper SK, Massoth G, Legendre P (1999). Physical and chemical factors
962 influencing species distributions on hydrothermal sulphide edifices of the Juan de Fuca
963 Ridge, Northeast Pacific. Marine Ecology Progress Series 190:89-112.
964
965 Sarrazin J, Walter C, Sarradin PM, Brind'Amour A, Desbruyères D, Briand P, Fabri MC, van
966 Gaever S, Vanreusel A, Bachraty C, Thiébaut E (2006). Community structure and
967 temperature dynamics within a mussel community on the southern East Pacific Rise. Cahiers
968 de Biologie Marine 47:483–490.
969
970 Sarrazin J, Blandin J, Delauney L, Dentrecolas S, Dorval P, Dupont J, Legrand J et al. (2007).
971 TEMPO: A new ecological module for studying deep-sea community dynamics at
972 hydrothermal vents. Paper presented at OCEANS '07 IEEE, Aberdeen, June 2007.
973 Proceedings no. 061215-042.
974
975 Scheirer DS, Shank TM, Fornari DJ (2006). Temperature variations at diffuse and focused
976 flow hydrothermal vent sites along the northern East Pacific Rise. Geochemistry Geophysics
977 Geosystems 7: Q03002; doi: 10.1029/2005GC001094.
978

979 Schöne BR, Giere O (2005). Growth increments and stable isotope variation in shells of the
980 deep-sea hydrothermal vent bivalve mollusk Bathymodiolus brevior from the North Fiji
981 Basin, Pacific Ocean. Deep Sea Res Part I 52:1896–1910.
982
983 Schultz A, Elderfield H (1997). Controls on the physics and chemistry of seafloor
984 hydrothermal circulation, Philosophical Transactions of the Royal Society London, 355:387-
985 425; doi:10.1098/rsta.1997.0014 1471-2962.
986
987 Sen A, Becker EL, Podowski EL, Wickes LN, Ma S, Mullaugh KM, Hourdez S, Luther GW III,
988 Fisher CR (2013). Hydrothermal vent chimney megafaunal communities on the Eastern Lau
989 Spreading Center and Valu Fa Ridge. Deep-Sea Research I 72:48-60.
990
991 Segonzac M (1992). Les peuplements associés à l'hydrothermalisme océanique du Snake Pit
992 (dorsale médio-Atlantique, 23°N, 3480m): composition et microdistribution de la
993 mégafaune. Compte-Rendus de l'Académie des Sciences Paris. 314:593-600.
994
995 Segonzac M, De Saint-Laurent M, Casanova B (1993). L'énigme du comportement trophique
996 des crevettes Alvinocarididae des sites hydrothermaux de la dorsale médio-atlantique.
997 Cahiers de Biologie Marine 34:535-571.
998
999 Shank TM, Fornari DJ, Von Damm KL, Lilley MD, Haymon RM, Lutz RA (1998). Temporal and
1000 spatial patterns of biological community development at nascent deep-sea hydrothermal
1001 vent (9°50'N, East Pacific Rise). Deep-Sea Research II 45:465-515; doi: 10.1016/S0967-
1002 0645(97)00089-1.

Shank T, Fornari DJ, Yoerger DR, Humphris SE, Bradley AL, Hammond S, Lupton JE, Scheirer D, Collier R, Reysenbach AL, Ding K, Seyfried W, Butterfield DA, Olson EJ, Lilley MD, Ward ME, Eisen JA (2003). Deep submergence synergy: Alvin and Abe explore the Galapagos Rift at 86°W. Eos, Transactions, American Geophysical Union 84:425-440.

Sievert SM, Ziebis W, Kuever J, Sahm K (2000). Relative abundance of Archaea and Bacteria along a thermal gradient quantified by rRNA slot-blot hybridization at a shallow-water hydrothermal vent. Microbiology 146:1287-1293.

Tivey MK, Bradley AM, Joyce TM, Kadko D (2002). Insights into tide-related variability at seafloor hydrothermal vents from time-series temperature measurements. Earth and Planetary Science Letters 202:693–707; doi:10.1016/S0012-821X(02)00801-4.

Tokeshi M (2011). Spatial structures of hydrothermal vents and vent-associated megafauna in the back-arc basin system of the Okinawa Trough, western Pacific. Journal of Oceanography 67:651-665; doi:10.1007/s10872-011-0065-9.

Tsurumi M, Tunnicliffe V (2001). Characteristics of a hydrothermal vent assemblage on a volcanically active segment of Juan de Fuca Ridge, northeast Pacific. Canadian Journal of Fisheries and Aquatic Sciences, 58:530-542; doi:10.1139/cjfas-58-3-530.

Tunnicliffe V (1991). The biology of hydrothermal vents: ecology and evolution. Oceanogr. Mar. Biol. Annu. Rev. M. Barnes, Aberdeen University Press. 29: 319-407.

Tunnicliffe V, Juniper SK (1990). Dynamic character of the hydrothermal vent habitat and the nature of sulphide chimney fauna. Progress in Oceanography 24:1–13.

Tunnicliffe V, Garrett JF and Johnson HP (1990). Factors affecting the mortality and behaviour of hydrothermal vent tube-worms (vestimentiferans). Deep-Sea Research 37: 103-125.

Tunnicliffe V, Embley RW, Holden JF, Butterfield DA, Massoth GJ and Juniper SK (1997). Biological colonization of new hydrothermal vents following an eruption on Juan de Fuca Ridge. Deep-Sea Research I 44: 1627-1644.

Van Dover CL (1995). Ecology of Mid-Atlantic Ridge hydrothermal vents. In: Parson LM, Walker CL, Dixon DR (eds) Hydrothermal Vents and Processes, Special Publication 87. Geological Society, London, pp. 257–294.

Van Dover CL, Desbruyères D, Segonzac M, Comtet T, Saldanha L, Fiala-Medioni A, Langmuir C (1996). Biology of the Lucky Strike hydrothermal field. Deep-Sea Research I 43:1509-1529.

Vuillemin R, LeRoux D, Dorval JP, Bucas K, Sudreau JP, Hamon M, LeGall C, Sarradin PM (2009). CHEMINI: A new *in situ* CHEmical MINIaturized analyser. Deep-Sea Research I 56:1391–1399; doi:10.1016/j.dsr.2009.02.002.

Table 1. Extraction of faunal and environmental data from the video footage recorded by the TEMPO module for 48 days (04/09/2006-22/10/2006) at ~1692 m depth at the base of the Eiffel Tower edifice (Lucky Strike vent field, Mid-Atlantic Ridge). The total studied surface covered approximately 0.1 m^2. Minimum and maximum values obtained for each temporal analysis are reported.

Faunal data	**Species**	**Treatment**	**Results (min & max)**
Abundance	*Bathymodiolus azoricus* *Pseudorimula midatlantica*	1 still image twice a day (A.M., P.M.)	40 to 52 individuals 0 to 8 individuals
	Mirocaris fortunata	5 still images twice a day (A.M., P.M.) 10 x 20 sec. video recordings (5 A.M., 5 P.M.)	2 to 27 individuals
	Segonzacia mesatlantica	4 min video recording twice a day (A.M., P.M.)	0 to 3 individuals
Valve opening	*Bathymodiolus azoricus*	5 still images twice a day (A.M., P.M.)	16 to 53% of the individuals
Changes in valve opening		22 x 4 min video recordings	Caused by passage of other species (37.8%) or unobserved events (62.2%)
Microbial cover		1 still image every 5 days x 10	27.47 to 34.53%
Environmental data	**Speed in cm sec^{-1}**	**Treatment**	**Results (min & max)**
Horizontal (current) and vertical (fluid flow) estimates in ordered classes			
1 2 … 10	0-1.49 1.5-2.49 … 9.5-10.49	4 min video sequence twice a day (A.M., P.M.)	0 to 10.5 cm sec^{-1} for the current 0 to 7.5 cm sec^{-1} for the fluid flow

A.M. morning; P.M. evening

Table 2. Long-term changes in faunal and microbial abundances at the TEMPO site located at the base of the Eiffel Tower edifice (~1692 m) between 2006 and 2008 based on analyses of still images. The wide-angle views of the studied assemblage were assembled out of photographs taken by the ROV while the close-up views correspond to still images recorded by the TEMPO camera.

Taxon	Wide angle				Close-up			
	2006		2008		2006		2008	
	Abundance	Density (ind m^{-2})	Abundance	Density (ind m^{-2})	Abundance	Density (ind m^{-2})	Abundance	Density (ind m^{-2})
Bathymodiolus azoricus	734	739.5	768	879.7	51	508.5	75	782.1
Mirocaris fortunata	42	42.3	27	30.9	24	239.3	9	93.8
Segonzacia mesatlantica	6	6.0	3	3.4	2	19.9	0	0.00
	cm^2	%	cm^2	%	cm^2	%	cm^2	%
Microbial cover	4068.1	41.0	3933.8	45.1	371.6	37.1	354.1	36.9
Mussel cover	2618.5	26.4	3265.4	37.4	239.7	23.9	345.0	36.0
Total surface (cm^2)	9925.5		8729.9		1002.6		959.1	

- Relative stability of the vent mussel assemblage in relation with abiotic conditions
- Hydrothermal habitats significantly influenced by ocean tidal signals
- Temporal variations in species abundance observed
- No established links between faunal abundance (except for shrimp) and environmental variables
- Direct species interactions not frequently observed

Figures

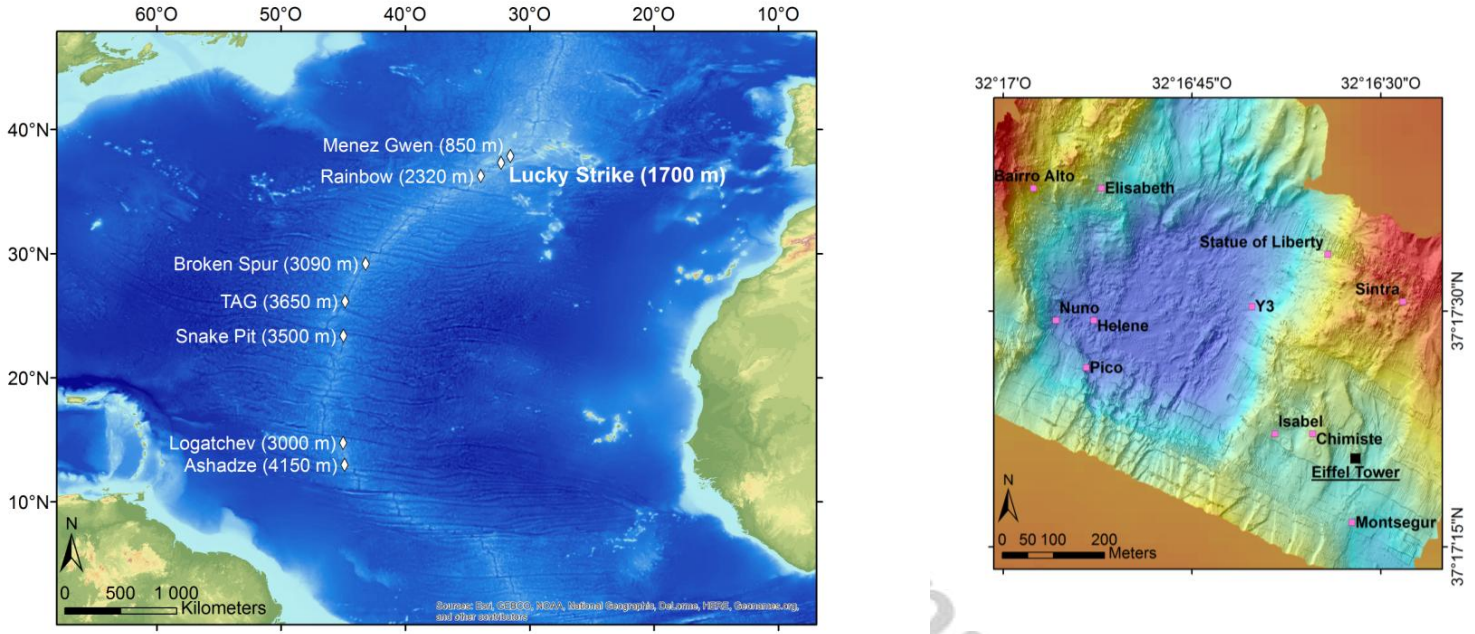

Figure 1. Location of the Lucky Strike vent field on the Mid-Atlantic Ridge at 37°17.59 N, 32°169 W. Data from the MNT ETOPO1 bedrock. The inset shows the hydrothermal vent field with several active sulphide edifices around a central lava lake, including the Eiffel Tower edifice in the south-east. Data from Ondreas et al., 2009.

Figure 2. The study scene as viewed by the TEMPO ecological observatory module at ~1692m depth at the base of the Eiffel Tower edifice (Lucky Strike vent field, MAR). TEMPO was deployed in 2006 during the MoMARETO cruise and recovered in 2008 during the MoMAR08 cruise. The CHEMINI sample inlet and associated temperature probe can be seen on the left-hand side of the picture. The total studied surface covered approximately 0.1 m^2.

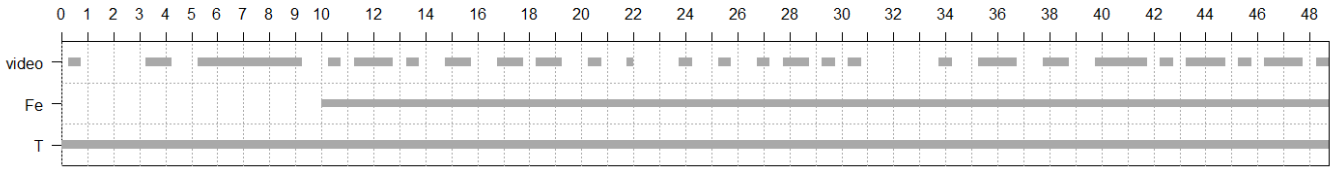

Figure 3. Overview of data (video, iron concentrations (Fe) and temperature (T)) available for the duration of the video recording. Days are indicated on the top axis. The 48 day time-series was done between 04/09/2006 to 22/10/2006.

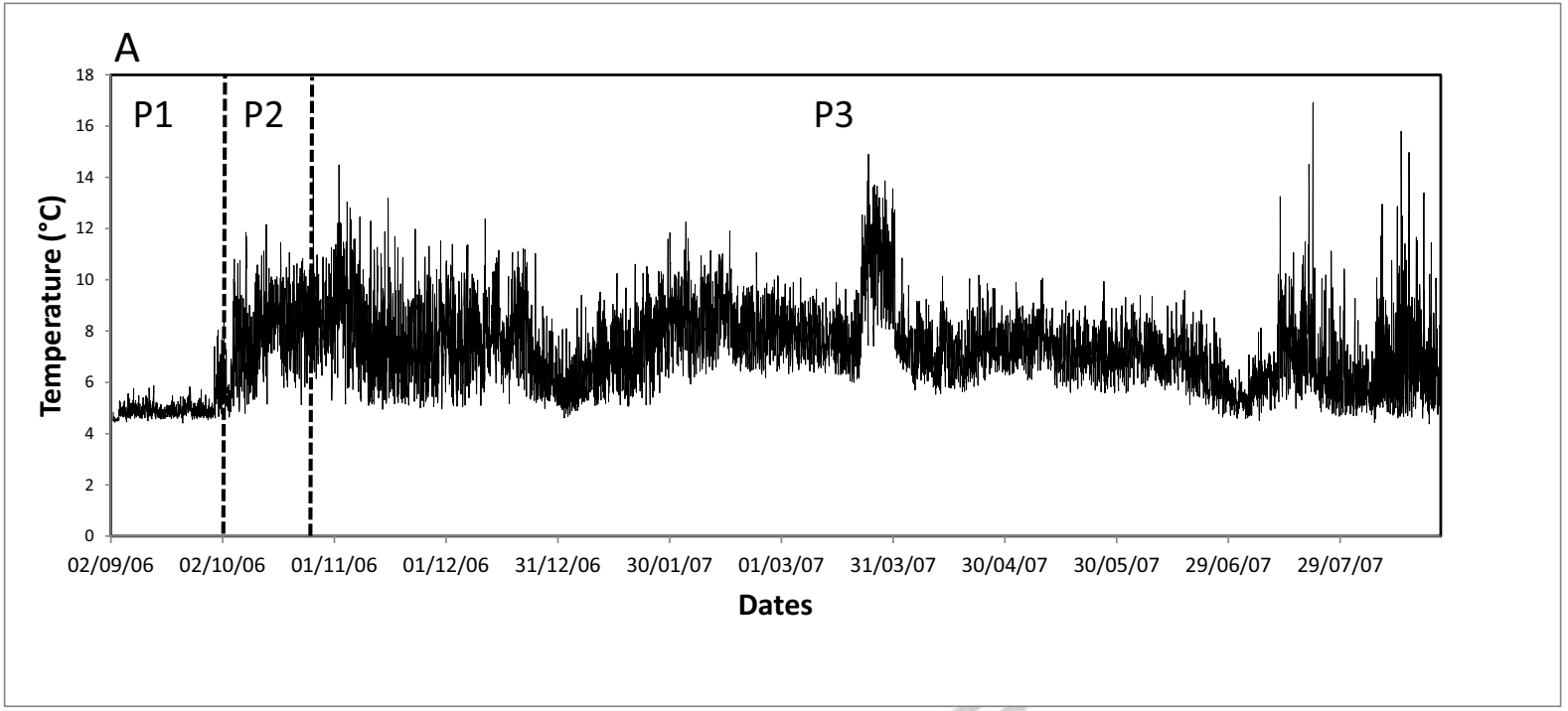

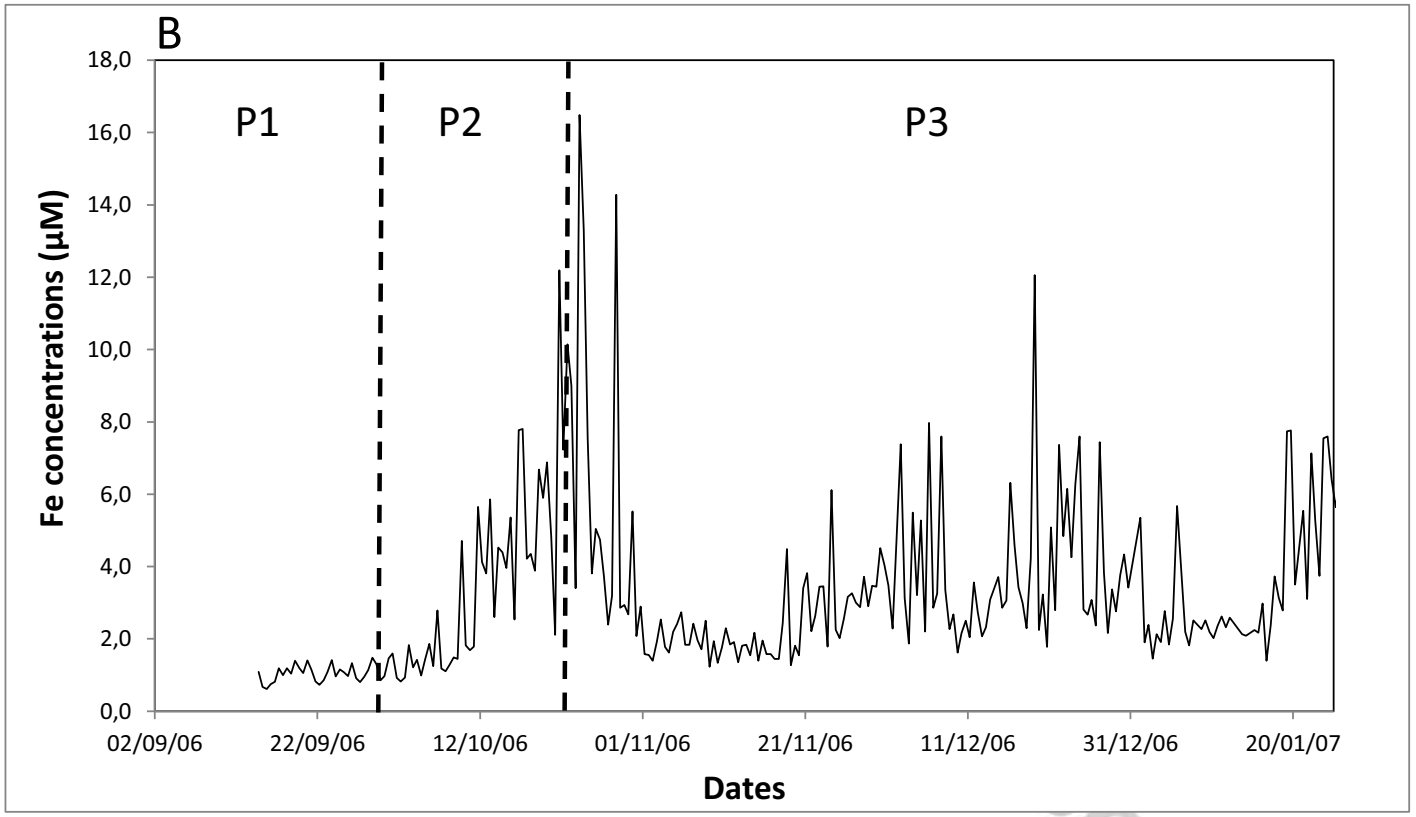

Figure 4. Overview of the temperature (A) and Fe (B) data available and analysed. P1 represents the values measured on the *Bathymodiolus azoricus* mussel assemblage before probe displacement (day 0 to 25 for T°C and day 10 to 25 for Fe, indicated by the dotted line), P2 represents the remaining period for which video imagery was available (day 26 to 48) while P3 corresponds to the rest of the time series (day 48 to 405 for T°C and day 48 to 143 for Fe). The temperature series in (A) is 405 days long (04/09/2006 to 14/10/2007, 9720 h) and the Fe series in (B) is 133 days long (14/09/2006 to 25/01/2007, 3192 h).

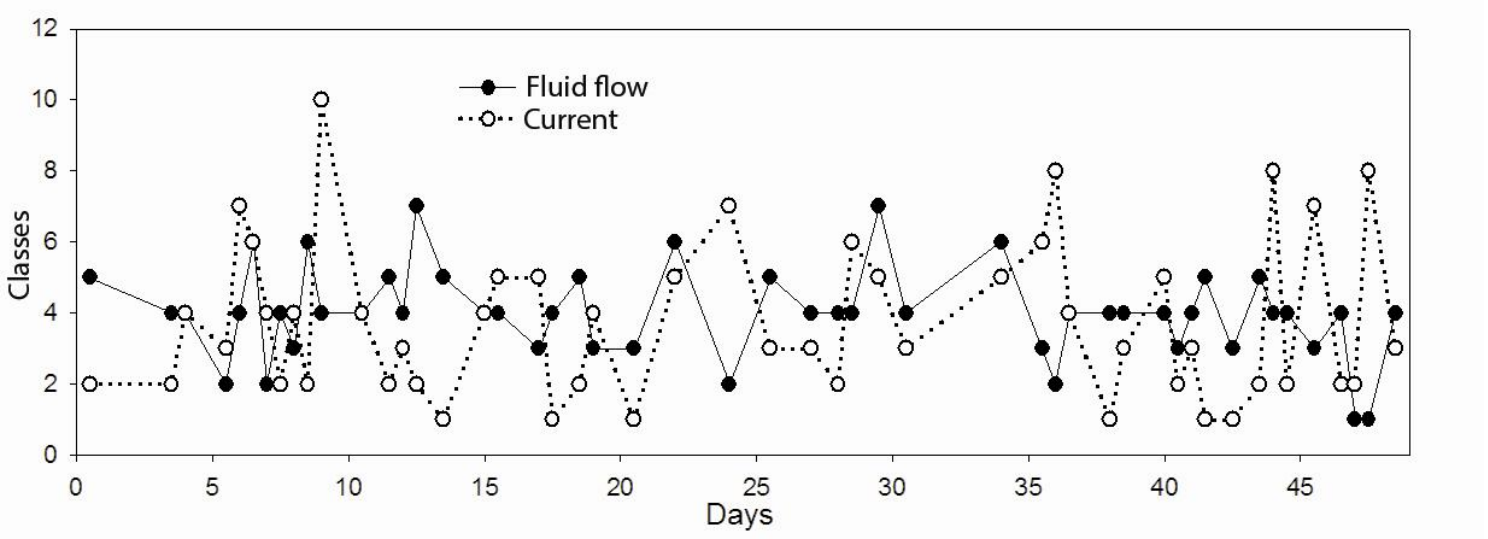

Figure 5. Vertical (fluid flow) and horizontal (current) components of water movement measured through on-screen particle tracking, and then put classified into different classes (see Table 1 for details) based on the velocities observed during P1 (day 0-25) & P2 (day 26-48).

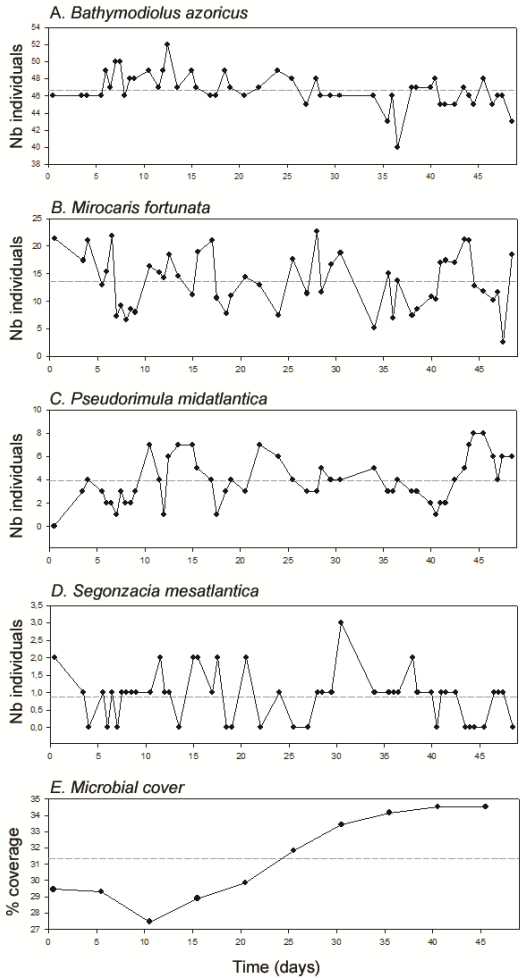

Figure 6. Variation in faunal abundances (A) *Bathymodiolus azoricus*, (B) *Mirocaris fortunata*, (C) *Pseudorimula midatlantica*, (D) *Segonzacia mesatlantica* and microbial coverage (E) as analysed from the video sequences, over the 48 days of video recording.

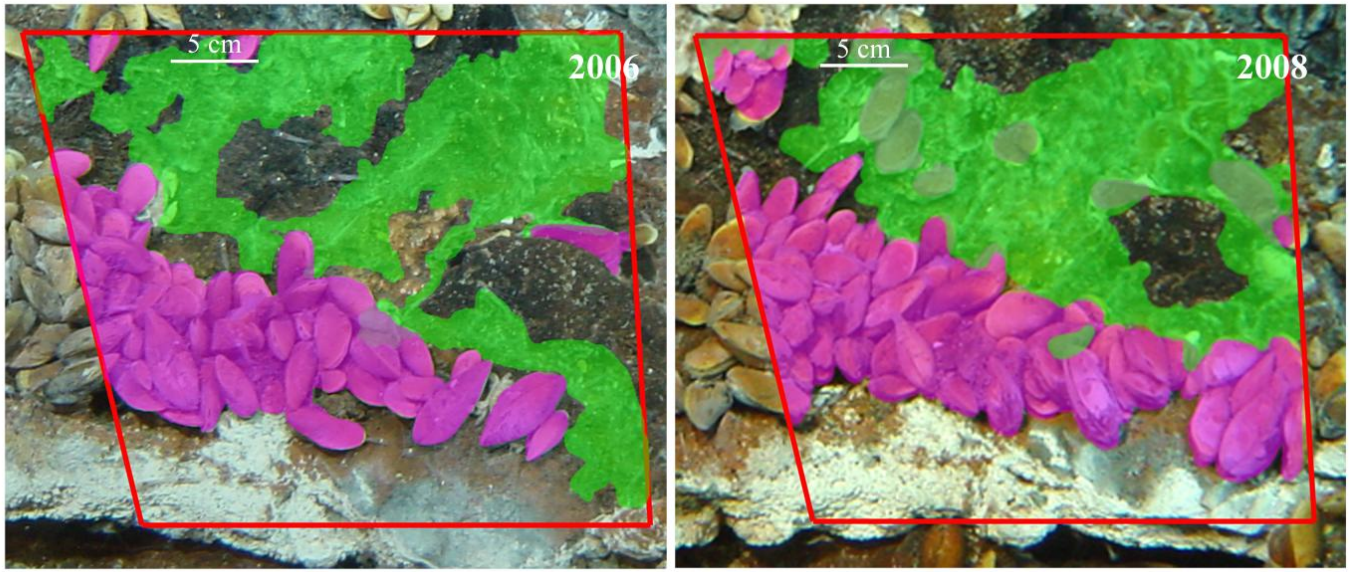

Figure 7. Faunal coverage in 2006 and 2008 as observed on the close-ups. The red trapezoid-shape represents the camera view of TEMPO. The mussels are coloured in pink and the microbial mats are highlighted in green.

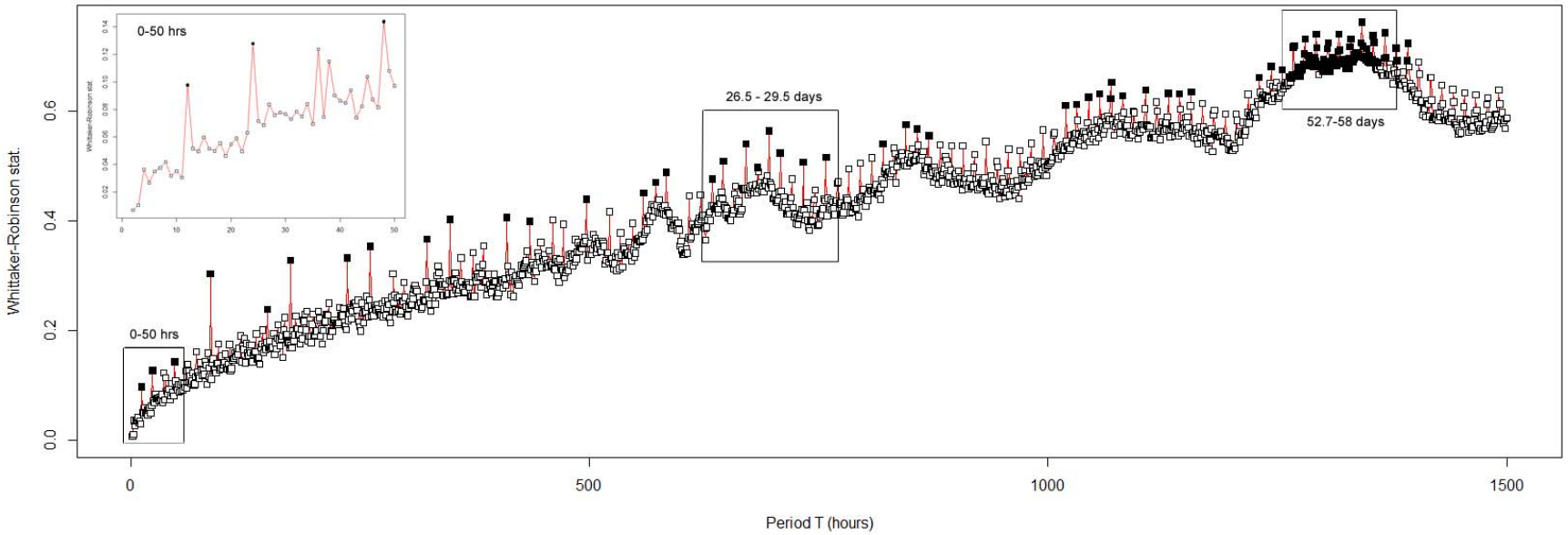

Figure 8. Whittaker-Robinson periodogram computed for temperature, featuring periods comprised between 2 and 1500 hours (approximately two months). Black squares indicate periods that are significant at the 5% level.

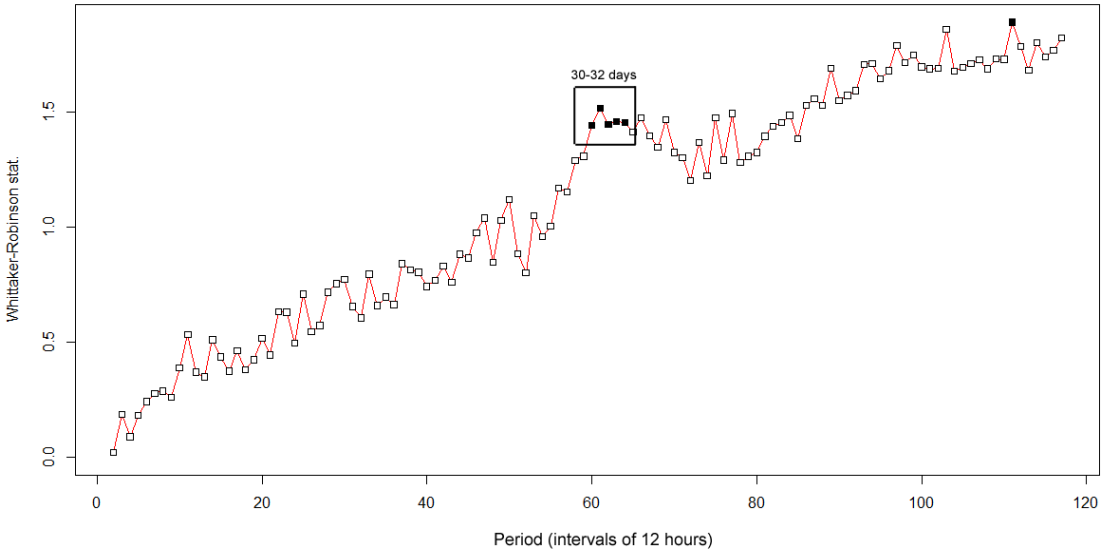

Figure 9. Whittaker-Robinson periodogram computed for Fe concentrations measured at 12 h intervals for 117 days, featuring periods comprised between 2 and 117 time intervals of 12h. The limit of the observation window of periodograms is the number of observation intervals divided by 2. Black squares indicate periods significant at the 5% level.